





ARTICLE

<https://doi.org/10.1038/s42004-019-0173-9>

OPEN

Low-temperature selective oxidation of methane over distant binuclear cationic centers in zeolites

Edyta Tabor ¹, Mariia Lemishka^{1,2}, Zdenek Sobalik¹, Kinga Mlekodaj ¹, Prokopis C. Andrikopoulos ¹, Jiri Dedecek¹ & Stepan Sklenak ¹

Highly active oxygen capable to selectively oxidize methane to methanol at low temperature can be prepared in transition-metal cation exchanged zeolites. Here we show that the α -oxygen stabilized by the negative charges of two framework aluminum atoms can be prepared by the dissociation of nitrous oxide over distant binuclear cation structures (M(II)...M(II), M = cobalt, nickel, and iron) accommodated in two adjacent 6-rings forming cationic sites in the ferrierite zeolite. This α -oxygen species is analogous to that known only for iron exchanged zeolites. In contrast to divalent iron cations, only binuclear divalent cobalt cationic structures and not isolated divalent cobalt cations are active. Created methoxy moieties are easily protonated to yield methanol, formaldehyde, and formic acid which are desorbed to the gas phase without the aid of water vapor while previous studies showed that highly stable methoxy groups were formed on isolated iron cations in iron exchanged ZSM-5 zeolites.

¹J. Heyrovsky Institute of Physical Chemistry, the Czech Academy of Sciences, Dolejskova 3, 18223 Prague, Czech Republic. ²Department of Physical Chemistry, Faculty of Chemical Technology, University of Pardubice, Namesti Cs. legii 565, 530 10 Pardubice, Czech Republic. Correspondence and requests for materials should be addressed to S.S. (email: stepan.sklenak@jh-inst.cas.cz)

The selective oxidation of methane represents one of the greatest challenges in catalysis and chemical technology, and therefore, attracts enormous attention. On the one hand, the selective oxidation of methane represents a promising way of the transformation of natural and shale gases into more valuable key chemical feedstocks with an enormous possible economic impact. On the other hand, the very high energy barrier of the incorporation of oxygen into the C–H bond of methane followed by significantly lower energy barriers of the subsequent oxidation steps in the total oxidation of methane to CO₂ and water make the selective oxidation of methane very difficult.

One of the key factors in this process is the formation of the highly reactive atomic oxygen which allows a decrease of the reaction temperature to prevent the total oxidation of methanol. The N₂O dissociation over Fe cations located in extra-framework cationic positions in zeolites is one possible route to prepare such a highly reactive atomic oxygen. The formation of the α -oxygen in Fe-zeolites and the successive selective oxidation of methane to methanol was firstly reported by Panov et al.¹ The structure of [Fe = O]²⁺ is suggested to be balanced by the negative charges of two AlO₄⁻ tetrahedra located in the ring of the zeolite framework which creates an extra-framework cationic site for divalent cations^{2,3} and only recently has been experimentally confirmed by Snyder et al. for Fe-BEA⁴ and Bols et al. for Fe-SSZ-13⁵. The selective oxidation of methane by N₂O is connected with several obstacles. One of them is the necessity of water or water-organic medium (e.g., acetonitrile, dimethyl ether) extraction of methoxy groups strongly bound to the catalyst^{6–12}.

Furthermore, the formation of the α -oxygen and the subsequent oxidation of methane to methanol has been reported to the best of our knowledge only for Fe-zeolites^{6,7,9,10,13}. This can be explained by the fact that the N₂O decomposition over other M(II)-zeolites occurs at such high temperatures (250–450 °C) that the reaction of the α -oxygen with N₂O occurs (i.e., formation of nitrates) or the creation of molecular oxygen prevails. Moreover, high activities of Fe(II) exchanged catalysts featuring the α -oxygen regarding the selective oxidation of methane were reported only for a limited number of topologies of iron-exchanged silicon rich zeolites (ZSM-5^{1,6,7,9,10,14,15}, ferrierite^{2,3}, SSZ-13⁵, and BEA^{4,16}).

During the last three decades, Panov et al. have studied catalysts containing isolated Fe(II) cations featuring the α -oxygen after their oxidation^{1,6,9,10,14,15}. The Fe(II) exchanged zeolite samples are treated at high temperatures reaching up to 900 °C^{6,9}. However, Panov et al. neither prepared the α -oxygen on a different M(II) cation than Fe(II) nor synthesized Fe(II) exchanged zeolites with binuclear cationic centers. Moreover, the Fe catalysts are difficult to prepare and the Fe centers are not stable under the preparation and reaction conditions. Furthermore, the selective oxidation of methane by the α -oxygen on Fe-zeolites is terminated after the formation of methoxy groups strongly bound to the catalyst, and subsequently, a water or water-organic medium extraction of the methoxy groups is necessary to liberate the oxidation products of methane from the catalyst^{9,10}.

There is another class of catalysts for selective oxidation of CH₄ which is copper exchanged zeolites^{8,11,12}. These materials are firstly activated in oxygen at 450–500 °C, and then cooled to 200 °C and react with methane in the absence of oxygen, thus protecting a methanol precursor from overoxidation. Subsequently, methanol can be extracted with water^{11,12}. After the oxidation, these Cu exchanged zeolites do not feature the “genuine” α -oxygen as defined by Panov et al.¹ and the structure of the oxidized active site does not correspond to that determined by Snyder et al.⁴, but it rather relates to a variant of Cu dimers or trimers^{8,11,12}.

Recently, a very high activity concerning the N₂O decomposition was reported for Fe(II) cations in the ferrierite zeolite. The studies showed^{2,3} that two Fe(II) cations accommodated in two adjacent 6-rings in the 8-ring channel (i.e., two adjacent β sites) of Fe-ferrierite (the calculated Fe–Fe distance is 7.4 Å) form the active site responsible for the superior activity of Fe-ferrierite in the N₂O decomposition. The DFT calculations³ showed that the cooperation of two adjacent Fe(II) cations caused a significant lowering of the energy barrier of the N₂O decomposition. This result raises a question if the cooperation of pairs of other transition metal M(II) cations can also significantly facilitate the abstraction of the oxygen atom from N₂O to yield the highly active α -oxygen. To answer this question, the ferrierite zeolite used in our prior studies^{2,3,17} was employed since it features a high concentration of two adjacent β sites³.

Here, we show the preparation of catalysts with new type of the reaction centers, specifically, distant binuclear structures of two transition metal M(II) cations (Co, Ni, and Fe) in the ferrierite matrix. The employment of these active sites overcome main obstacles connected with the isolated Fe(II) cations. Our investigation reveals that the preparation of the α -oxygen on M(II) cations other than Fe(II) brings significant advantages concerning the stability of M(II) cations and their possible high concentrations in zeolite matrices. In addition, these M(II)-zeolites can be prepared using simpler procedures and milder conditions by ion exchange (Co(II)) and impregnation (Ni(II)), followed by a consequent calcination at 450 °C, and not by a complex way at high temperatures as Panov et al.¹ and Snyder et al.⁴ used. Moreover, the variability of the type of the cation forming the binuclear active sites can potentially lead to catalysts with different catalytic properties. Furthermore, our study shows that the selective oxidation of methane over the binuclear sites does not terminate after the formation of methoxy groups strongly bound to the catalyst. Conversely, the oxidation yields mainly methanol and formaldehyde, and therefore, the extraction step is not needed.

Results

DFT calculations. The possible activity of binuclear cation M(II) structures in the abstraction of O from N₂O and the subsequent formation of the α -oxygen was investigated by periodic DFT calculations for Co(II) and Fe(II) cations. The calculations were performed for a model with two M(II) cations accommodated in two adjacent β sites of ferrierite³ corresponding to the fully ion exchanged ferrierite zeolite with M(II) cations. The computed mechanisms are the same for both Co(II) and Fe(II). Only the results for Co(II) are described in detail (Fig. 1) while those computed for Fe(II) are discussed in detail in our prior study³ (see Supplementary Table 1) which however used another DFT functional and different technical settings (details are in Section electronic structure calculations).

Therefore, the results for Fe(II) were recalculated to allow the direct comparison of the computational results for Co(II) with those for Fe(II).

Firstly, N₂O adsorbs by the terminal N atom to create a [Co...NNO Co] complex (2) in which the O atom of N₂O is well positioned to attack the bare Co(II) cation in the adjacent β site. The calculated adsorption energy is –15.4 kcal/mol (–16.1 kcal/mol for Fe(II)-ferrierite). Consequently, the N–O bond is cleaved and the bare Co(II) cation in the adjacent β site is oxidized to yield a [Co...NN O=Co] intermediate (3) via the [Co-NNO-Co] transition state (TS). The corresponding computed barrier is 25.0 kcal/mol. This value indicates that the oxidation of Co(II) to give the α -oxygen should be facile but significantly more sluggish than the same reaction step on Fe(II)-ferrierite (i.e., the barrier

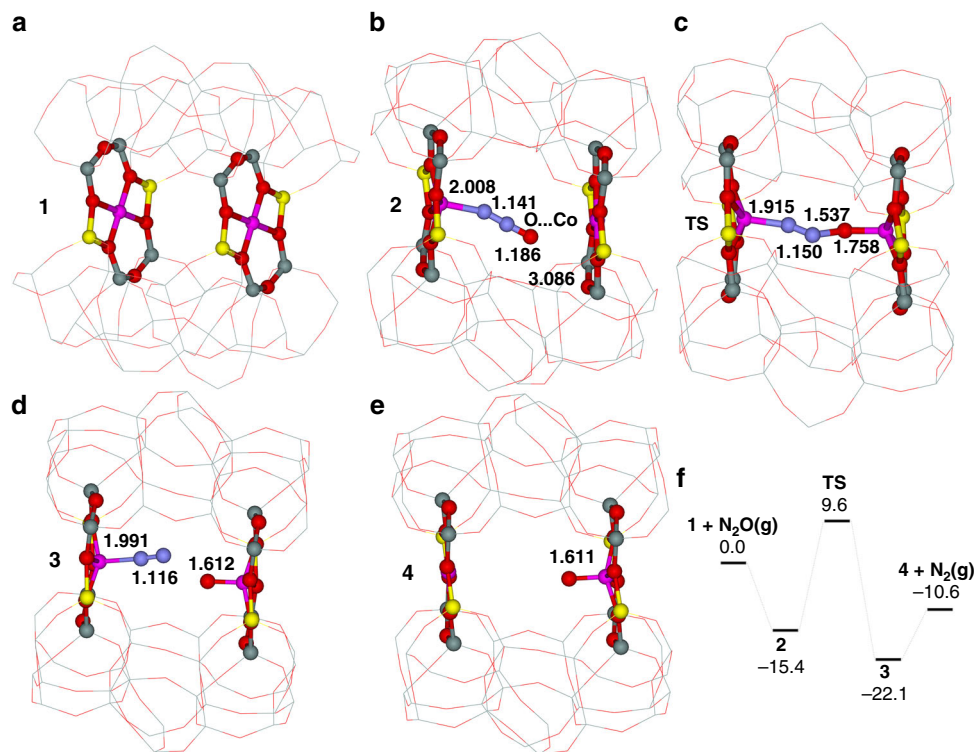


Fig. 1 Optimized structures. **a** The two adjacent β sites of Co-ferrierite **1** after molecular dynamics simulations. **b** The Co...NNO Co complex **2** formed in the two adjacent β sites. **c** The transition state **TS** created in the two adjacent β sites. **d** The Co...NN O=Co intermediate **3** formed in the two adjacent β sites. **e** The Co O=Co product **4** created in the two adjacent β sites. The distances are in Å. Silicon atoms are in gray, oxygen atoms in red, aluminum atoms in yellow, cobalt atoms in violet, and nitrogen atoms in blue. Schematic energy profile (in kcal mol⁻¹) **f** The formation of the α -oxygen

of 14.5 kcal/mol). The calculated energy for this reaction step is -6.7 kcal/mol (-14.2 kcal/mol for Fe(II)-ferrierite). Subsequently, N_2 desorbs, which costs 11.5 kcal/mol (12.5 kcal/mol for Fe(II)-ferrierite), and the [Co O=Co] product (**4**) featuring the α -oxygen is formed. Furthermore, our calculations reveal that N_2O does not adsorb on Co(II) by the oxygen atom indicating that the α -oxygen cannot be created on isolated Co(II) cations.

Distant binuclear M(II) cationic centers. The formation of distant binuclear M(II) cationic centers in zeolites requires fulfilling three conditions. (i) The presence of two adjacent 6-rings or 8-rings able to form cationic sites for bare divalent cations. The two adjacent rings must face each other. (ii) Each of the two rings has to contain two Al atoms (i.e., four Al atoms in total). The two rings, therefore, can form two adjacent cationic sites for bare divalent cations. (iii) The occupation of the two adjacent cationic sites by two divalent cations. Various reactions on distant binuclear M(II) cationic centers require different optimal distances between the two adjacent cations.

Two adjacent 6-rings creating the β sites in the 8-ring channel of M(II)-ferrierite (the calculated M–M distance is ca 7.4 Å) are candidates to form the distant binuclear M(II) cationic centers. The Si/Al ratio of the ferrierite sample^{3,17} is 8.6 meaning that there are in average 3.75 Al atoms per unit cell. The prior study showed that the concentration of Al pairs in the β site is high (50% of all the Al atoms)¹⁷ so ca. 94% of the 6-rings of the β site can accommodate bare divalent cations. Therefore, at least 88% (0.94×2) of the β sites are able to form binuclear M(II) structures³. The investigated Co(II)-ferrierite and Ni(II)-ferrierite are ion exchanged ($M/Al \geq 0.25$) close to the maximum loading of bare divalent cations (M/Al 0.33)¹⁷. Therefore, almost all the β sites are occupied and binuclear M(II) cationic species are unambiguously formed. Assuming the worst-case scenario that all

other cationic sites are occupied by M(II) before the formation of the binuclear species, it is guaranteed that at least 50% of M(II) cations are in the form of the binuclear species when $M/Al > 0.22$ ¹⁷. Conversely, Fe(II) cations were introduced into the ferrierite sample using acetylacetonate^{2,3,18}. This procedure guarantees the creation of binuclear Fe(II) structures in all occupied β sites even at the lowest Fe loadings Fe/Al 0.04 employed to prevent the formation of Fe-oxidic species^{2,3,18,19}.

Dissociation of N_2O over distant binuclear cations. The computational results (Fig. 1) show that this ferrierite zeolite can serve for the preparation of the α -oxygen on Co-zeolites. Therefore, we experimentally tested our theoretical predictions regarding Co(II) using the same ferrierite parent zeolite as that employed in the prior studies^{2,3,17}. In addition, another divalent transition metal cation Ni(II), which was not calculated for technical reasons, was investigated as well. Moreover, Fe(II)-ferrierite as well as a second Fe(II)-ferrierite sample, containing isotopically enriched ⁵⁷Fe (i.e., ⁵⁷Fe(II)-ferrierite) used for Mössbauer spectroscopy experiments, were explored for comparison. Furthermore, we also investigated the nature of the α -oxygen formed on the Co(II)-ferrierite, Ni(II)-ferrierite, and Fe(II)-ferrierite samples. The selective oxidation of methane was used as a test of the α -oxygen.

FTIR spectroscopy of bare divalent cations. FTIR spectroscopy of the shifted antisymmetric T-O-T stretching vibrations of the lattice induced by binding bare Co(II) cations to the framework oxygens was employed to investigate the formation of the α -oxygen and its activity in the oxidation reactions. This method allows analysis of (i) bare divalent cations accommodated in the individual cationic sites and (ii) the formations of complexes of divalent cations with guest molecules^{2,19–24}.

Although the structure of the α -oxygen in Fe-zeolite was recently analyzed by the combination of various spectroscopies supported by quantum chemical calculations⁴, the α -oxygen on Fe is defined as the active oxygen species formed by the N₂O oxidation and capable to oxidize hydrogen, CO¹, benzene^{25,26}, and methane^{1,27}. Moreover, the unambiguous spectroscopic characterization of the α -oxygen on other transition metal cations than Fe by the approach reported by Snyder et al.⁴, would represent a daunting task, so the confirmation of the oxidation activity of the α -oxygen species is essential. Methane represents a test molecule of the first choice due to the economic importance of the selective oxidation of CH₄, and moreover, the requirement of testing the high activity of the α -oxygen for selective oxidations. In addition, analysis of the FTIR spectra measured after the interaction of the oxidized M-zeolite with methane allows the detection of the oxygen-containing products.

The FTIR spectra in the region of the shifted antisymmetric T–O–T stretching lattice modes (Fig. 2) confirmed (i) the presence of bare Co(II), Ni(II), and Fe(II) cations in the ferrierite matrix, (ii) the interaction of all the three M(II) cations with N₂O at ambient temperature and at 200 °C, and (iii) the successive interaction with methane at ambient temperature and at 200 °C.

Mössbauer spectroscopy experiments. Mössbauer spectroscopy was used for analysis of the oxidation state and the coordination of the Fe species in the ⁵⁷Fe-ferrierite sample and to support the interpretations of the FTIR spectra. Mössbauer spectra of the ⁵⁷Fe-ferrierite sample recorded under the same conditions as the FTIR ones are shown in Fig. 3, and the corresponding Mössbauer parameters are listed in Table 1.

FTIR spectroscopy of cations after the interaction with N₂O.

The FTIR spectra of the M-ferrierite samples evacuated at 450 °C exhibited two main bands in the region of the shifted antisymmetric T–O–T stretching lattice modes at around 940 and 920 cm⁻¹, which confirm the presence of M(II) cations in the α and β cationic sites, respectively (Fig. 2). The shifted antisymmetric T–O–T stretching vibrations describe the redox behavior of the M species. FTIR spectroscopy of the evacuated samples revealed that the M(II) cations accommodated in ferrierite are predominantly located in the β site for all the three M-ferrierite samples. In addition, Mössbauer spectroscopy of the ⁵⁷Fe-ferrierite matrix confirmed the presence of Fe in the α and β sites as well (Table 1 and Fig. 3).

The FTIR measurements of the interaction of N₂O with the evacuated samples at ambient temperature (0.5–14 min) (the spectra (i) in Fig. 4) and after the desorption at 200 °C for 5 min

(the spectra (ii) in Fig. 4) reveal a disappearance of the bands of the M(II) cations in the β cationic positions, and furthermore, a formation of two new bands at ca 950 and ca 880 cm⁻¹.

The former band can be attributed to the ligand complex M(II) with N₂O²² while the latter band, which is weaker, indicates the increase of the cation–zeolite interaction and can be attributed to the [Me=O]²⁺ complex featuring the α -oxygen analogously to the Fe-ferrierite¹⁹. The newly formed species corresponding to the band at about 880 cm⁻¹ is resistant to an evacuation at 200 °C for 5 min (the spectra (ii) in Fig. 4). The formation of the α -oxygen in the ⁵⁷Fe-ferrierite sample is observed in the Mössbauer spectrum as well (Table 1). The corresponding Mössbauer parameters have been already reported^{4,19,28}. Note that the formation of the α -oxygen for M-zeolite (M=Co and Ni) with a low M loading (i.e., M/Al ~ 0.1) was not observed although the ratios (α/β) of the occupations of the α and β sites by M(II) were similar to those of the highly exchanged M(II)-ferrierites. Conversely, the α -oxygen is created in the Fe-ferrierite sample with the Fe/Al ratio of 0.04 since the procedure of the introduction of Fe(II)^{3,18} guarantees the creation of binuclear Fe(II) structures in all occupied β sites even at this very low Fe(II) loading.

The interactions of N₂O with the evacuated M(II)-samples were investigated by FTIR at ambient temperature and 200 °C (Fig. 4) to compare the reactivity of the three M(II) pairs in the formation of the α -oxygen. The intensity of the band at around 880 cm⁻¹ corresponding to the α -oxygen formed over the Fe-sample reached its steady state in 4 min while it took 6 and 14 min for the Co-ferrierite and Ni-ferrierite samples, respectively, to achieve the steady state. It should be noted that the α -oxygen is not the final product of the reaction.

Study of the nature of the α -oxygen. The α -oxygen formed on the M(II)-ferrierite samples was investigated employing the selective oxidation of methane monitored by FTIR spectroscopy (Fig. 5).

The M(II)-zeolites were oxidized by N₂O at ambient temperature for 4–14 min, followed by the N₂O desorption at 200 °C for 5 min (the spectra (i) in Fig. 5) and consequently methane was introduced and reacted with the α -oxygen at ambient temperature for 1 min (the spectra (ii) in Fig. 5) and at 200 °C for 25 min (the spectra (iii) in Fig. 5). The FTIR spectra (the spectra (i), (ii), and (iii) in Fig. 5) clearly reveal a decrease of the intensity of the bands at around 880 cm⁻¹ corresponding to the α -oxygen.

Analysis of the FTIR spectra (Fig. 6) in the region of the C–H stretching band (3000–2830 cm⁻¹) recorded after 25 min of the

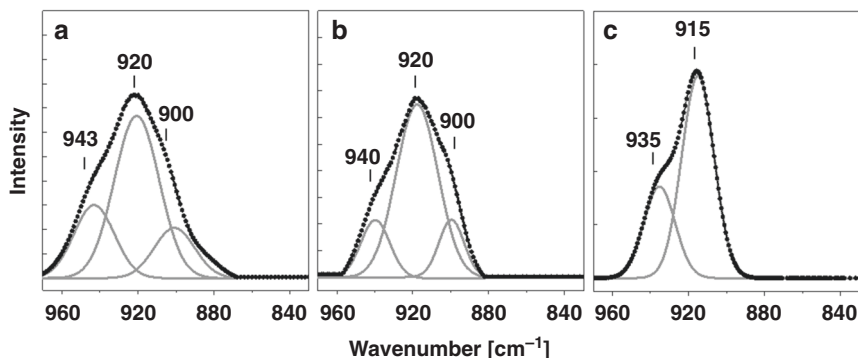


Fig. 2 FTIR T–O–T spectra of the M-ferrierites. **a** Co-ferrierite. **b** Ni-ferrierite. **c** Fe-ferrierite. The samples are evacuated at 450 °C for 3 h. The bands at 943, 940, and 935 cm⁻¹ correspond to Co(II), Ni(II), and Fe(II) cations, respectively, accommodated in the α site. The wavenumbers at 920, 920, and 915 cm⁻¹ relate to Co(II), Ni(II), and Fe(II) cations, respectively, bound in the β site. The bands at 900 cm⁻¹ are linked with the γ sites in Co-ferrierite and Ni-ferrierite, while this cationic site is not occupied in Fe-ferrierite due to the low Fe/Al ratio. The tick mark labels on the y-axis are at 0.0, 0.2, 0.4, ...

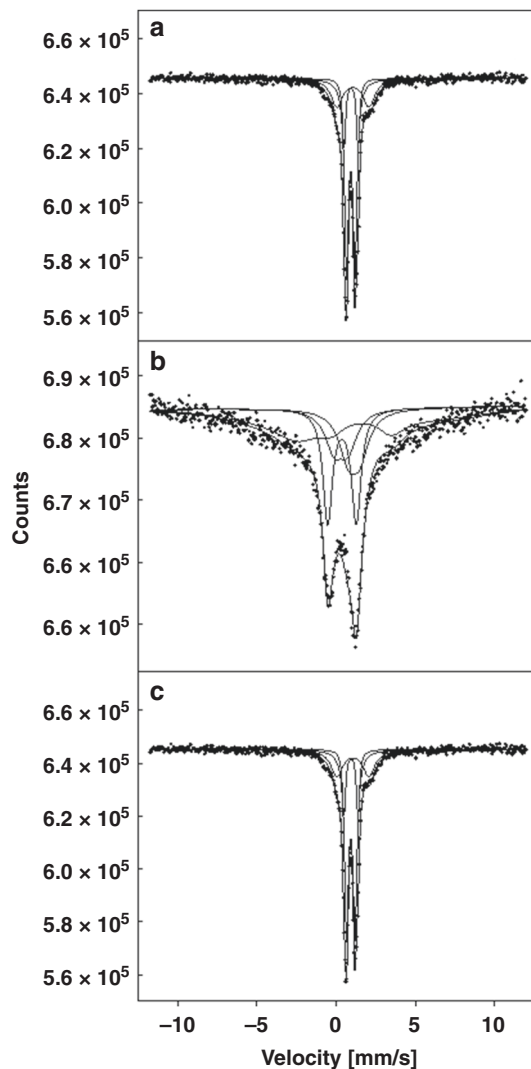


Fig. 3 Mössbauer spectra with their fits of ^{57}Fe -ferrierite. **a** ^{57}Fe -ferrierite after the following treatment: 3 h evacuation at 450 °C for 3 h. **b** ^{57}Fe -ferrierite after the following treatment: an evacuation at 450 °C for 3 h then an interaction with N_2O (40 Pa) at 200 °C for 30 min and after that a N_2O desorption at 200 °C for 5 min. **c** ^{57}Fe -ferrierite after the following treatment: an evacuation at 450 °C for 3 h, then an interaction with N_2O (40 Pa) for 30 min at 200 °C, and subsequently, a N_2O desorption at 200 °C for 5 min, and after that a CH_4 (40 Pa) adsorption for 30 min at 200 °C, and subsequently, a CH_4 desorption at ambient temperature

interaction with methane at 200 °C reveals the presence of the band at 2960 cm^{-1} corresponding to formate species bound to the iron cation, the band at 2853 cm^{-1} attributed to CH_3OH , and the band at 2920 cm^{-1} which is assigned to methoxy group bound to the iron cation (Fig. 6a–c)^{7,10,13}.

Bands in the region of δCH_3 , δCOH , and νCO vibrations ($1800\text{--}1290\text{ cm}^{-1}$) appear at (i) 1666 and 1355 cm^{-1} assigned to formate anions bound to the iron cation and (ii) 1642 cm^{-1} attributed to formaldehyde adsorbed on the iron cation (Fig. 6a–c)¹³. It should be stressed that although the FTIR spectra recorded after methane oxidation over the M-ferrierites feature bands of similarly low intensity as those already reported for Fe-ZSM-5 under similar conditions^{7,10}, the former spectra are significantly more complex due to the formation of a wide range of oxidation products on the M-ferrierites. The presence of the bands characterizing methanol, formaldehyde, and formate indicate that the protonation of methoxy groups in the

Table 1 The parameters of the Mössbauer spectra

Fe-FER Fe/Al 0.04	IS mm/s	QS mm/s	B_{fit} T	Rel. %	Fe species	Fe(II)/Fe(III)
Evacuated @ 450 °C	0.98	0.49	46	35	Fe(II)	100/0
	1.00	0.78		40	Fe(II)	
	1.05	2.10		25	Fe(II)	
+ N_2O @ 200 °C	1.12	0.71	20	Fe(II)	20/80	
	0.31	0.88	15	Fe(III)		
	0.37	1.80	25	Fe(III)		
	0.53	–	46	Fe(III)		
+ $\text{N}_2\text{O}/\text{CH}_4$ @ 200 °C	0.98	0.49	46	35	Fe(II)	100/0
	0.95	0.78		40	Fe(II)	
	1.05	2.10		25	Fe(II)	

The Mössbauer parameters and the spectral contributions of Fe species of the dehydrated ^{57}Fe -ferrierite, the ^{57}Fe -ferrierite after the interaction with N_2O , and the ^{57}Fe -ferrierite after the interaction with N_2O and CH_4

M-ferrierites with binuclear M(II) species is more facile compared to isolated Fe(II) cations in Fe-ZSM-5 for which only methoxy species were recognized in the FTIR spectra^{7,10}. Therefore, an extraction by water steam was required to obtain methanol from Fe-ZSM-5^{7,10}. Conversely, the presence of methanol and other oxidation products indicates that such an extraction may not be needed for all the three investigated M-ferrierite samples. This fact is further confirmed by FTIR spectra of all the three M-ferrierites recorded after the interaction with methane at 200 °C and the successive evacuation at 200 °C. The FTIR spectra reveal (i) complete disappearance of the band at ca 880 cm^{-1} corresponding to the α -oxygen and (ii) the reappearance of the band at around 920 cm^{-1} characterizing bare M(II) cations accommodated in the β site (the spectra (iv) in Fig. 5). It should be noted that the α -oxygen is stable during the desorption at 200 °C for 5 min (spectra (ii) in Fig. 4). Therefore, the emergence of the band at about 920 cm^{-1} which characterizes bare divalent cations located in the β site further indicates the protonation of methoxy groups, and subsequently, the formation of volatile products of the oxidation of methane and confirms the identification of the products of methane oxidation in the FTIR spectra. This conclusion is further supported for the ^{57}Fe -ferrierite sample by Mössbauer spectroscopy (Table 1 and Fig. 3c) which evidences the predominant presence of bare Fe(II) cations with the parameters identical with those observed for the evacuated ^{57}Fe -ferrierite sample before the oxidation by N_2O . The above reported higher protonation activity of all the three M-ferrierite samples (i) results in the creation of the protonated oxidation products (i.e., methanol, formaldehyde, and formic acid) and (ii) can be explained by a higher activity of the ferrierite zeolite to form protonated adducts²⁹.

A titration of the α -oxygen by methane was performed by through-flow experiment with the products of methane oxidation monitored by a quadrupole mass spectrometer to confirm the protonation of methoxy groups and to elucidate the composition of the products of the oxidation of methane. All the three M-ferrierite samples (i.e., M=Co, Ni, and Fe) after the activation in helium were oxidized by N_2O at 200 °C. Then, the formed α -oxygen was titrated by methane at the same temperature. The formations of methanol ($m/z = 31$), other possible products ($m/z = 29$) of the oxidation of methane (i.e., formaldehyde, formic acid, and dimethyl ether), and CO_2 ($m/z = 44$) were monitored by mass spectrometry (Fig. 6). The yields of the produced methanol per gram of zeolite are listed in Table 2. The amount of formaldehyde, formic acid, and dimethyl ether all together per one M(II) cation was estimated to be less than ca 0.04 mol/mol_M and only traces of CO_2 were observed. The

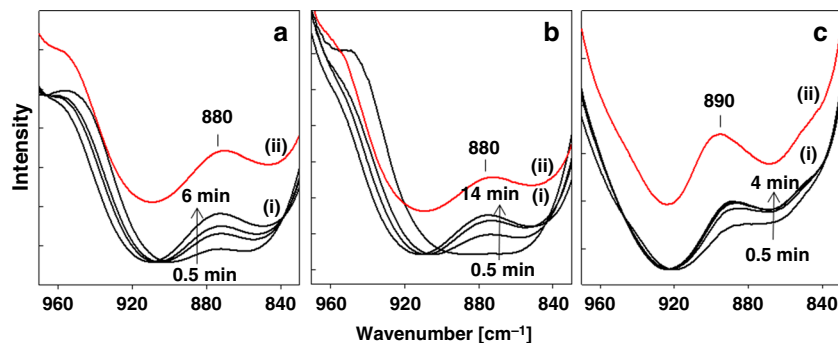


Fig. 4 FTIR T–O–T spectra of the oxidized M-ferrites. **a** Co-ferrite. **b** Ni-ferrite. **c** Fe-ferrite. The M-ferrite samples interact with N₂O at ambient temperature for 0.5–14 min (i). The spectra after the subsequent desorption of N₂O at 200 °C for 5 min (ii). The tick mark labels on the y-axis are at 0.0, 0.2, 0.4, ...

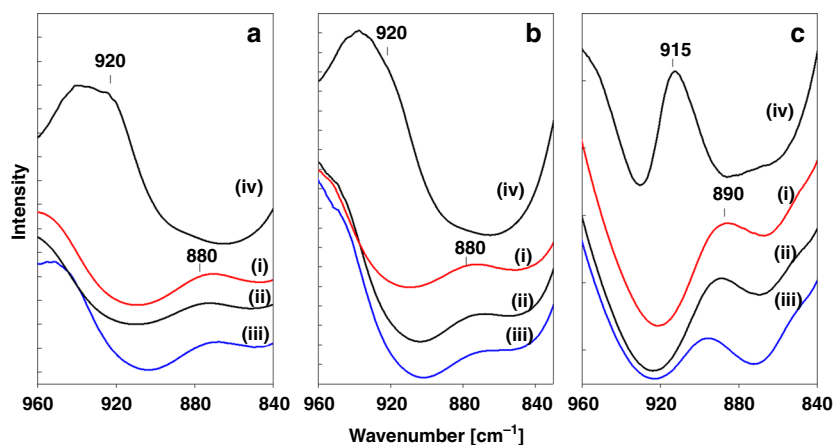


Fig. 5 FTIR T–O–T spectra the oxidized and reduced M-ferrites. **a** Co-ferrite. **b** Ni-ferrite. **c** Fe-ferrite. The M-ferrite samples after the desorption of N₂O at 200 °C for 5 min (i), the interaction with CH₄ at ambient temperature for 1 min (ii), the interaction with CH₄ at 200 °C for 25 min (iii), the desorption of CH₄ at 200 °C for 5 min (iv). The tick mark labels on the y-axis are at 0.0, 0.2, 0.4, ...

production of methanol related to one M(II) cation (Table 2) did not exceed 0.5 mol_{CH₃OH}/mol_{M_e}. This result further confirms that the active sites for the formation of the α -oxygen and methanol oxidation represent two cooperating M(II) cations.

Discussion

The α -oxygen with notable oxidation properties can be prepared not only on a Fe(II)-zeolite but also on a zeolite exchanged with two other divalent cations—Co(II) and Ni(II). The variability of the type of the cation forming the distant binuclear active sites can potentially allow the tuning of the corresponding catalytic properties. The α -oxygen is formed over all the three M(II)-ferrite samples (M=Co(II), Ni(II), and Fe(II)) by the abstraction of the oxygen atom from N₂O by pairs of transition metal M(II) cations. Two M(II) cations accommodated in two adjacent 6-rings in the 8-ring channel (i.e., β sites) of M(II)-ferrite create the binuclear active site responsible for the formation of the α -oxygen. The α -oxygen is then able to selectively oxidize methane mainly to methanol. The protonation of methoxy groups to yield methanol and other oxidation products occurs spontaneously without using water steam in contrast to all the previously reported zeolite-based systems. This difference makes the extraction of the oxidation products very easy since the products desorb from the M(II)-zeolite to the gas phase. Only distant binuclear Co(II)...Co(II) structures and not isolated Co(II) cations are active in the formation of the α -oxygen while both the types of Fe(II) cations are potent to yield the α -oxygen.

Methods

Sample preparation and treatment. Commercially supplied ferrite Si/Al 8.6 (Tosoh Company, Japan) was ion exchanged (3 \times 24 h, ambient temperature, 100 ml of solution/1 g of zeolite) with 1 M NH₄NO₃, washed by distilled water and dried at ambient temperature to prepare the NH₄ form of ferrite.

The Fe(II)-ferrite catalyst was prepared by the impregnation of NH₄-ferrite by acetylacetonate solution of FeCl₃. Then, the sample was evacuated for 1 h at 100 °C and consequently for 3 h at 350 °C. After cooling to ambient temperature, the sample was washed with distilled water and calcined overnight under air flow at 420 °C. The preparation procedure is described in details elsewhere^{2,3,18,19}. The ⁵⁷Fe(II)-ferrite zeolite with Fe/Al 0.04 for Mössbauer spectroscopy measurements was prepared by the same procedure using isotopically enriched ⁵⁷FeCl₃.

Two Co(II)-ferrite samples were prepared by ion exchange with a 0.05 M solution of Co(NO₃)₂·6H₂O at 60 °C (3 \times 24 h to obtain the high Co(II) concentration and 1 \times 24 h to get the low Co(II) concentration, 100 ml of solution/1 g of zeolite). After the ion exchange, the zeolites were thoroughly washed and dried in air at ambient temperature.

Ni(II) was introduced to ferrite using the dry impregnation technique to yield the Ni(II)-ferrite sample with the high Ni/Al ratio^{30,31}. The sample was granulated and dehydrated for 4 h at 120 °C. 0.2 g Ni(NO₃)₂·6H₂O was dissolved in 1.0 g water and added dropwise to the zeolite. The sample was subsequently dried on air for 24 h at ambient temperature, then calcined in air at 450 °C for 4 h. Conversely, an ion exchange with 0.05 M solution of Ni(NO₃)₂ at ambient temperature (2 \times 24 h, 100 ml of solution/1 g of zeolite) was employed to give the Ni-ferrite sample with the low Ni/Al ratio.

All the M-ferrite samples were characterized by chemical analysis to obtain the M/Al values (Fe/Al 0.04, Co/Al 0.25 and 0.13, Ni/Al 0.28 and 0.08).

Mössbauer spectroscopy. Mössbauer spectroscopic measurements were performed using self-supporting pellets of ⁵⁷Fe-ferrite. The Mössbauer spectra were recorded at ambient temperature under dynamic vacuum (10⁻³ Pa) after:

- (i) an evacuation at 450 °C for 3 h;

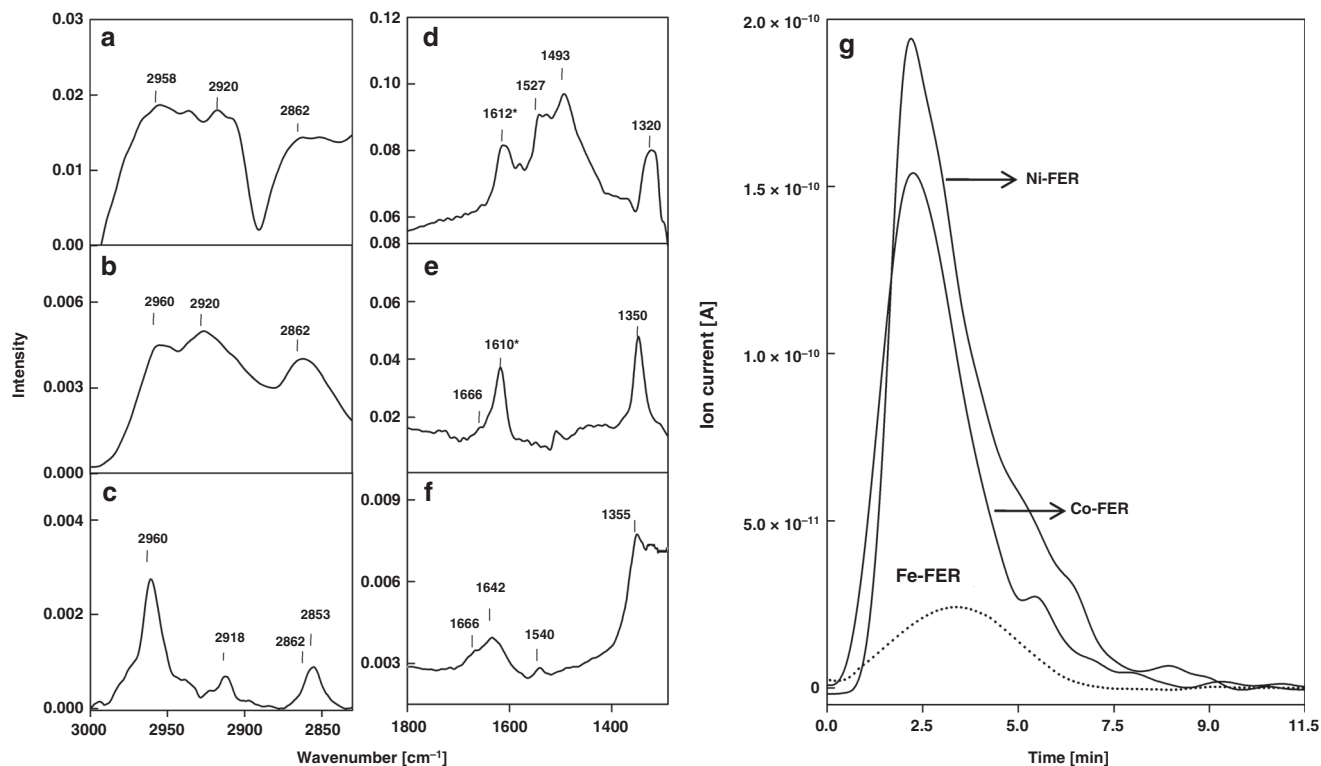


Fig. 6 FTIR spectra of the M-ferriferite samples. **a** Co-ferriferite. **b** Ni-ferriferite. **c** Fe-ferriferite. **d** Co-ferriferite. **e** Ni-ferriferite. **f** Fe-ferriferite. The spectra are shown in the regions 3000–2830 cm^{-1} and 1800–1290 cm^{-1} . The spectra are recorded after the interaction of the M-ferriferite samples with N_2O at 200 °C for 25 min followed by the 5 min N_2O desorption at 200 °C, and the subsequent interaction with CH_4 at 200 °C for 10 min. **g** The mass spectrometry results for the Co-ferriferite, Ni-ferriferite, and Fe-ferriferite. Methanol was detected after the oxidation of the samples by N_2O at 200 °C and then the formed α -oxygen was titrated by methane at the same temperature. The *band in the region 1600–1621 cm^{-1} represents the bending mode of adsorbed water¹³

Table 2 Chemical composition of the studied M-ferriferite samples

M-FER	Si/Al	M/Al	Yield of CH_3OH $\mu\text{mol/g}_{\text{cat}}$	$\text{CH}_3\text{OH}/\text{Me}$ mol/mol
Co-FER	8.6	0.25	200	0.24
Co-FER	8.6	0.13	0	–
Ni-FER	8.6	0.28	290	0.32
Ni-FER	8.6	0.08	0	–
Fe-FER	8.6	0.04	32	0.21
^{57}Fe -FER	8.6	0.04	–	–
Fe-CHA ⁵	10.1	0.03	27	0.68

- (ii) an evacuation at 450 °C for 3 h, then an interaction with N_2O (40 Pa) for 30 min at 200 °C and after that a N_2O desorption at 200 °C for 5 min;
 (iii) an evacuation at 450 °C for 3 h, then an interaction with N_2O (40 Pa) for 30 min at 200 °C, and consequently 5 min a N_2O desorption at 200 °C, and after that a CH_4 (40 Pa) adsorption for 30 min at 200 °C, and subsequently, a CH_4 desorption at ambient temperature.

The source of γ -rays was ^{57}Co in a rhodium matrix and the α -Fe foil was used as a reference. The spectra were deconvoluted into Lorentzian-shaped components using the MossWinn software³². The individual components were characterized by the isomer shift (IS) describing the oxidation state of the Fe species and the quadrupole splitting (QS) related to the Fe coordination. The assignment of the Mössbauer parameters to the Fe species in ^{57}Fe -ferriferite was based on our prior studies^{33–35}.

Infrared spectroscopy. Infrared spectra were recorded employing a Nicolet 6700 FTIR spectrometer (resolution 2 cm^{-1} , 32 scans/min) equipped with a liquid nitrogen cooled MCT-B detector and KBr windows. The samples in a form of self-supporting pellets (10 mg cm^{-2}) were placed in the cuvette allowing evacuation and dosing of gases. FTIR spectra of the M-ferriferite samples were recorded after the following treatments:

- (i) an evacuation at 450 °C for 3 h (Fig. 2);
 (ii) an evacuation at 450 °C for 3 h, then an interaction with N_2O (10^{-3} Pa) at ambient temperature for 0.5–14 min depending on the M(II) cation (the spectra (i) in Fig. 4);
 (iii) an evacuation at 450 °C for 3 h, then an interaction with N_2O (10^{-3} Pa) at ambient temperature for 4–14 min depending on the M(II) cation followed by a N_2O desorption at 200 °C for 5 min (the spectra (ii) in Fig. 4 and the spectra (i) in Fig. 5);
 (iv) an evacuation at 450 °C for 3 h, then an interaction with N_2O (10^{-3} Pa) at ambient temperature for 4–14 min depending on the M(II) cation, followed by a N_2O desorption at 200 °C for 5 min, and subsequently, an interaction with CH_4 (10^{-3} Pa) at ambient temperature for 1 min (the spectra (ii) in Fig. 5);
 (v) an evacuation at 450 °C for 3 h, then an interaction with N_2O (10^{-3} Pa) at ambient temperature for 4–14 min depending on the M(II) cation, followed by a N_2O desorption at 200 °C for 5 min, and subsequently, an interaction with CH_4 (10^{-3} Pa) at 200 °C for 25 min (the spectra (iii) in Fig. 5);
 (vi) an evacuation at 450 °C for 3 h, then an interaction with N_2O (10^{-3} Pa) at ambient temperature for 4–14 min depending on the M(II) cation, followed by a N_2O desorption at 200 °C for 5 min, than an interaction with CH_4 (10^{-3} Pa) at 200 °C for 25 min and a subsequent CH_4 desorption at 200 °C for 5 min (the spectra (iv) in Fig. 5).

The FTIR spectra of the oxidation products (Fig. 6) were corrected by background subtraction. Separate experiments were performed to collect the backgrounds. FTIR spectra of the M-ferriferite samples were recorded after following treatments: an evacuation at 450 °C for 3 h, then an interaction with CH_4 (10^{-3} Pa) at 200 °C for 25 min.

Mass spectrometry. The products of the titration of the α -oxygen by methane in the through-flow experiment were monitored by mass spectrometry (Balzers QMG 421C quadrupole mass spectrometer). The sample placed in the quartz reactor was activated in a flow of He (20 mL/min) for 3 h at 450 °C. Subsequently, the sample was treated in a flow of N_2O (40 mL/min; 3 vol. % in He) at 200 °C for 5 min followed by a purging with He (20 mL/min) for 5 min. Finally, the oxidized sample was left to interact with CH_4 (30 mL/min) at 200 °C for 10 min. The signals for $m/z = 31$ for methanol, $m/z = 29$ for other possible oxidation products (formaldehyde, formic acid, and dimethyl ether), and $m/z = 44$ for CO_2 were

monitored. The signal $m/z = 31$ was integrated and compared with calibration data for methanol to quantify the yield of methanol.

Computational models. Two models were employed for the Co(II) cation and one model for the Fe(II) cation. All the three models possess P1 symmetry and feature a super cell composed of two unit cells along the c dimension (i.e., $a = 18.651$, $b = 14.173$, and $c = 14.808$ Å). The Fe model and one Co model contain four Al/Si substitutions forming two β sites with the four Al atoms located in the T4 sites of the two adjacent 6-rings (only the β site with both Al in T4 was found in the ferrierite framework of this ferrierite sample¹⁷) accommodating two Fe(II) and two Co(II) cations, respectively. The two models serve to investigate the possible activity of binuclear cation M(II) structures. The other Co model contains two Al/Si substitutions forming one β sites with the two Al atoms located in the T4 sites of the 6-rings accommodating one Co(II) cation. This model is of use to study the possible activity of isolated Co(II) cations. The starting structure was generated from the experimental orthorhombic structure of ferrierite determined by neutron diffraction³⁶.

Electronic structure calculations. Periodic DFT calculations were carried out by employing the VASP code^{37–40}. The high-spin electron configurations $d5\uparrow d1\downarrow$ and $d5\uparrow d2\downarrow$ were employed for the Fe(II) and Co(II) cations, respectively, accommodated in the zeolite. The Kohn–Sham equations were solved variationally in a plane-wave basis set using the projector-augmented wave (PAW) method of Blöchl⁴¹, as adapted by Kresse and Joubert⁴². The exchange–correlation energy was described by the PBE generalized gradient approximation (GGA) functional⁴³. Brillouin zone sampling was restricted to the Γ point. A plane-wave cutoff of 600 eV and the dDsC dispersion correction^{44,45} were utilized for geometry optimizations and a smaller cutoff of 400 eV and the DFT-D2 method⁴⁶ were used for the molecular dynamics simulations.

The prior periodic DFT calculations on Fe(II)-ferrierite used the PW91 functional, lower plane-wave cutoffs of 400 eV (geometry optimizations) and 300 eV (molecular dynamics), and no dispersion correction³. Details are provided in Supplementary Note 1. However, the overall conclusions of the prior study and this investigation regarding Fe(II)-ferrierite remain the same³.

Molecular dynamics. The molecular dynamics (MD) simulations were carried out on all the three models. The MD computations used the exact Hellmann–Feynman forces acting on atoms and applied the statistics of canonical ensemble to the motion of the atomic nuclei⁴⁷ by using the Verlet velocity algorithm^{48,49} to integrate Newton’s equations of motion. The time step for the integration of the equations of motion was 1 fs. The simulations were run for 10,000 fs at 400 K. Visual inspection of the structures along the MD trajectories showed that the duration of the MD simulations was long enough, because it included both the rearrangements of the local structures of the ferrierite framework (up to ca. 2000 fs) as well as a long period (ca. 8000 fs) when the system fluctuated around the equilibrium and “snapshots” were collected and optimized. Similar time lengths were used for MD simulations of cationic sites in zeolites^{3,50–54}. The MD simulations serve to obtain the rearranged local structures (details are provided in our prior studies^{3,50}). The rearrangement can be monitored by visual inspection. No physical quantity is derived from the MD trajectories. The structures of twenty distinct “snapshots” collected at 500, 1000, 1500, ... 10,000 fs of the molecular dynamics simulations were optimized for the computational models. Additional details are provided in Supplementary Note 2.

Geometry optimizations. The collected “snapshots” were optimized. The atomic positions were optimized at constant volume by employing a conjugate-gradient algorithm minimization of energies and forces whereas the lattice parameters were fixed at their experimental values.

Data availability

The data that support the findings of this study are available within the paper. Other relevant data are available from the corresponding author upon reasonable request.

Received: 28 February 2019 Accepted: 31 May 2019

Published online: 21 June 2019

References

1. Panov, G. I., Sobolev, V. I. & Kharitonov, A. S. The role of iron in N₂O decomposition on ZSM-5 zeolite and reactivity of the surface oxygen formed. *J. Mol. Cat.* **61**, 85–97 (1990).
2. Jisa, K. et al. Role of the Fe-zeolite structure and iron state in the N₂O decomposition: comparison of Fe-FER, Fe-BEA, and Fe-MFI catalysts. *J. Catal.* **262**, 27–34 (2009).
3. Sklenak, S. et al. N₂O decomposition over Fe-zeolites: structure of the active sites and the origin of the distinct reactivity of Fe-ferrierite, Fe-ZSM-5, and Fe-beta. A combined periodic DFT and multispectral study. *J. Catal.* **272**, 262–274 (2010).
4. Snyder, B. E. R. et al. The active site of low-temperature methane hydroxylation in iron-containing zeolites. *Nature* **536**, 317–332 (2016).
5. Bols, M. L. et al. Spectroscopic identification of the α -Fe/ α -O active site in Fe-CHA zeolite for the low-temperature activation of the methane C-H bond. *J. Am. Chem. Soc.* **140**, 12021–12032 (2018).
6. Dubkov, K. A. et al. Kinetic isotope effects and mechanism of biomimetic oxidation of methane and benzene on FeZSM-5 zeolite. *J. Mol. Catal., A* **123**, 155–161 (1997).
7. Wood, B. R., Reimer, J. A., Bell, A. T., Janicke, M. T. & Ott, K. C. Methanol formation on Fe/Al-MFI via the oxidation of methane by nitrous oxide. *J. Catal.* **225**, 300–306 (2004).
8. Groothaert, M. H., Smeets, P. J., Sels, B. F., Jacobs, P. A. & Schoonheydt, R. A. Selective oxidation of methane by the bis(μ -oxo)dicopper core stabilized on ZSM-5 and mordenite zeolites. *J. Am. Chem. Soc.* **127**, 1394–1395 (2005).
9. Starokon, E. V., Parfenov, M. V., Pirutko, L. V., Abornev, S. I. & Panov, G. I. Room-temperature oxidation of methane by α -oxygen and extraction of products from the FeZSM-5 Surface. *J. Phys. Chem. C* **115**, 2155–2161 (2011).
10. Starokon, E. V. et al. Oxidation of methane to methanol on the surface of FeZSM-5 zeolite. *J. Catal.* **300**, 47–54 (2013).
11. Grundner, S. et al. Single-site trinuclear copper oxygen clusters in mordenite for selective conversion of methane to methanol. *Nat. Commun.* **6**, 7546 (2015).
12. Tomkins, P., Ranocchiaro, M. & van Bokhoven, J. A. Direct conversion of methane to methanol under mild conditions over Cu-zeolites and beyond. *Acc. Chem. Res.* **50**, 418–425 (2017).
13. Nobukawa, T. et al. In-situ observation of reaction intermediate in the selective catalytic reduction of N₂O with CH₄ over Fe ion-exchanged BEA zeolite catalyst for the elucidation of its reaction mechanism using FTIR. *J. Phys. Chem. B* **108**, 4071–4079 (2004).
14. Pirutko, L. V., Chernyavsky, V. S., Uriarte, A. K. & Panov, G. I. Oxidation of benzene to phenol by nitrous oxide: Activity of iron in zeolite matrices of various composition. *Appl. Catal., A* **227**, 143–157 (2002).
15. Pirutko, L. V. et al. The role of α -sites in N₂O decomposition over FeZSM-5. Comparison with the oxidation of benzene to phenol. *Appl. Catal., B* **91**, 174–179 (2009).
16. Centi, G., Genovese, C., Giordano, G., Katovic, A. & Perathoner, S. Performance of Fe-BEA catalysts for the selective hydroxylation of benzene with N₂O. *Catal. Today* **91-2**, 17–26 (2004).
17. Dedecek, J. et al. Complex analysis of the aluminum siting in the framework of silicon-rich zeolites. A case study on ferrierites. *J. Phys. Chem. C* **115**, 11056–11064 (2011).
18. Sobalik, Z., Wichterlova, B., Markvart, M. & Tvaruzkova, Z. *CZ Patent* 293917 B6 (2001).
19. Sobalik, Z., Tabor, E., Novakova, J., Sathu, N. K. & Zaveta, K. Role of active oxygen and NO_x species in N₂O decomposition over Fe-ferrierite. *J. Catal.* **289**, 164–170 (2012).
20. Jacobs, W., Vanwolput, J. & Vansanten, R. A. An insitu fourier-transform infrared study of zeolitic vibrations: dehydration, deammoniation, and reammoniation of ion-exchanged Y zeolites. *Zeolites* **13**, 170–182 (1993).
21. Lei, G. D., Adelman, B. J., Sarkany, J. & Sachtler, W. M. H. Identification of copper(II) and copper(I) and their interconversion in Cu/ZSM-5 de-NO_x catalysts. *Appl. Catal., B* **5**, 245–256 (1995).
22. Sobalik, Z., Tvaruzkova, Z. & Wichterlova, B. Skeletal T-O-T vibrations as a tool for characterization of divalent cation complexation in ferrierite. *J. Phys. Chem. B* **102**, 1077–1085 (1998).
23. Sobalik, Z., Tvaruzkova, Z. & Wichterlova, B. Monitoring of skeletal T-O-T vibrations of metal ion exchanged zeolites—an attempt at quantitative evaluation. *Microporous Mesoporous Mater.* **25**, 225–228 (1998).
24. Sobalik, Z., Dedecek, J., Ikonnikov, I. & Wichterlova, B. State and coordination of metal ions in high silica zeolites Incorporation, development and rearrangement during preparation and catalysis. *Microporous Mesoporous Mater.* **21**, 525–532 (1998).
25. Dubkov, K. A., Paukshtis, E. A. & Panov, G. I. Stoichiometry of oxidation reactions involving α -oxygen on FeZSM-5 zeolite. *Kinet. Catal.* **42**, 205–211 (2001).
26. Ivanov, D. P., Sobolev, V. I. & Panov, G. I. Deactivation by coking and regeneration of zeolite catalysts for benzene-to-phenol oxidation. *Appl. Catal., A* **241**, 113–121 (2003).
27. Dubkov, K. A., Sobolev, V. I. & Panov, G. I. Low-temperature oxidation of methane to methanol on FeZSM-5 zeolite. *Kinet. Catal.* **39**, 72–79 (1998).
28. Dubkov, K. A., Ovanesyan, N. S., Shteinman, A. A., Starokon, E. V. & Panov, G. I. Evolution of iron states and formation of α -sites upon activation of FeZSM-5 zeolites. *J. Catal.* **207**, 341–352 (2002).

29. Sazama, P., Tvaruzkova, Z., Jirglova, H. & Sobalik, Z. in *Zeolites and related materials: Trends, targets and challenges, proceedings of the 4th international Feza conference* Vol. 174 *Stud. Surf. Sci. Catal.* (eds A. Gedeon, P. Massiani, & F. Babonneau) 821–824 (Elsevier, Amsterdam, 2008).
30. Maia, A. J., Louis, B., Lam, Y. L. & Pereira, M. M. Ni-ZSM-5 catalysts: detailed characterization of metal sites for proper catalyst design. *J. Catal.* **269**, 103–109 (2010).
31. Gamliel, D. P. et al. Nickel impregnated mesoporous USY zeolites for hydrodeoxygenation of anisole. *Microporous Mesoporous Mater.* **261**, 18–28 (2018).
32. Klencsar, Z. MossWinn-methodological advances in the field of Mossbauer data analysis. *Hyperfine Interact.* **217**, 117–126 (2013).
33. Tabor, E., Zaveta, K., Sathu, N. K., Tvaruzkova, Z. & Sobalik, Z. Characterization of iron cationic sites in ferrierite using Mossbauer spectroscopy. *Catal. Today* **169**, 16–23 (2011).
34. Tabor, E. et al. N₂O decomposition over Fe-FER: A Mossbauer study of the active sites. *Catal. Today* **175**, 238–244 (2011).
35. Sazama, P. et al. Structure and critical function of Fe and acid sites in Fe-ZSM-5 in propane oxidative dehydrogenation with N₂O and N₂O decomposition. *J. Catal.* **299**, 188–203 (2013).
36. Pickering, I. J., Maddox, P. J., Thomas, J. M. & Cheetham, A. K. A neutron powder diffraction analysis of potassium-exchanged ferrierite. *J. Catal.* **119**, 261–265 (1989).
37. Kresse, G. & Hafner, J. Ab-initio molecular-dynamics for open-shell transition-metals. *Phys. Rev. B* **48**, 13115–13118 (1993).
38. Kresse, G. & Hafner, J. Ab-initio molecular-dynamics simulation of the liquid-metal amorphous-semiconductor transition in germanium. *Phys. Rev. B* **49**, 14251–14269 (1994).
39. Kresse, G. & Furthmuller, J. Efficient iterative schemes for ab initio total-energy calculations using a plane-wave basis set. *Phys. Rev. B* **54**, 11169–11186 (1996).
40. Kresse, G. & Furthmuller, J. Efficiency of ab-initio total energy calculations for metals and semiconductors using a plane-wave basis set. *Comput. Mater. Sci.* **6**, 15–50 (1996).
41. Blochl, P. E. Projector augmented-wave method. *Phys. Rev. B* **50**, 17953–17979 (1994).
42. Kresse, G. & Joubert, D. From ultrasoft pseudopotentials to the projector augmented-wave method. *Phys. Rev. B* **59**, 1758–1775 (1999).
43. Perdew, J. P., Burke, K. & Ernzerhof, M. Generalized gradient approximation made simple. *Phys. Rev. Lett.* **77**, 3865–3868 (1996).
44. Steinmann, S. N. & Corminboeuf, C. Comprehensive Bench marking of a density-dependent dispersion correction. *J. Chem. Theory Comput.* **7**, 3567–3577 (2011).
45. Steinmann, S. N. & Corminboeuf, C. A generalized-gradient approximation exchange hole model for dispersion coefficients. *J. Chem. Phys.* **134**, 044117 (2011).
46. Grimme, S. Accurate description of van der Waals complexes by density functional theory including empirical corrections. *J. Comput. Chem.* **25**, 1463–1473 (2004).
47. Nose, S. A unified formulation of the constant temperature molecular-dynamics methods. *J. Chem. Phys.* **81**, 511–519 (1984).
48. Verlet, L. Computer experiments on classical fluids. I. Thermodynamical properties of Lennard-Jones molecules. *Phys. Rev.* **159**, 98–103 (1967).
49. Verlet, L. Computer experiments on classical fluids. II. Equilibrium correlation functions. *Phys. Rev.* **165**, 201–214 (1968).
50. Sklenak, S. et al. Effect of the Al Siting on the structure of Co(II) and Cu(II) cationic sites in ferrierite. A periodic DFT molecular dynamics and FTIR study. *J. Phys. Chem. C* **117**, 3958–3968 (2013).
51. Klein, P. et al. NMR crystallography of monovalent cations in inorganic matrixes: Li⁺ siting and the local structure of Li⁺ sites in ferrierites. *Chem. Commun.* **51**, 8962–8965 (2015).
52. Sazama, P. et al. Al-rich beta zeolites. Distribution of Al atoms in the framework and related protonic and metal-ion species. *J. Catal.* **333**, 102–114 (2016).
53. Karcz, R. et al. TNU-9 zeolite: aluminum distribution and extra-framework sites of divalent cations. *Chem. Eur. J.* **23**, 8857–8870 (2017).
54. Mlekodaj, K. et al. Al organization in the SSZ-13 zeolite. Al distribution and extraframework sites of divalent cations. *J. Phys. Chem. C* **123**, 7968–7987 (2019).

Acknowledgements

This work was supported by the Grant Agency of the Czech Republic under projects: # 17-00742S and the RVO: 61388955 and by Czech Academy of Sciences under Strategy AV21 (Program Molecules and Materials for Life). The DFT calculations were supported by The Ministry of Education, Youth, and Sports from the Large Infrastructures for Research, Experimental Development and Innovations project, “IT4Innovations National Science Center—LM2015070”. Chemical analyses of samples were provided in the frame of CATPRO (Ministry of Education, Youth and Sports, ref. no. MSMT-1000/2016, under Project No. LM2015039), which has been integrated into the National Program for Sustainability I of the Ministry of Education, Youth and Sports of the Czech Republic through the project Development of the UniCRE Centre, Project Code LO1606.

Author contributions

S.S. and P.C.A. carried out the DFT calculations. E.T., K.M., Z.S. and M.L. performed the FTIR measurements. J.D. and S.S. supervised the progress of the entire project. J.D. and E.T. designed all the experiments. M.L. and E.T. prepared the zeolite samples. E.T. and K.M. carried out the mass spectrometry experiments. All the authors contributed to the discussion regarding various aspects of the project. The paper was written through collective contributions from all authors. All authors approved the final version of the manuscript.

Additional information

Supplementary information accompanies this paper at <https://doi.org/10.1038/s42004-019-0173-9>.

Competing interests: The authors declare no competing interests.

Reprints and permission information is available online at <http://npg.nature.com/reprintsandpermissions/>

Publisher's note: Springer Nature remains neutral with regard to jurisdictional claims in published maps and institutional affiliations.



Open Access This article is licensed under a Creative Commons Attribution 4.0 International License, which permits use, sharing, adaptation, distribution and reproduction in any medium or format, as long as you give appropriate credit to the original author(s) and the source, provide a link to the Creative Commons license, and indicate if changes were made. The images or other third party material in this article are included in the article's Creative Commons license, unless indicated otherwise in a credit line to the material. If material is not included in the article's Creative Commons license and your intended use is not permitted by statutory regulation or exceeds the permitted use, you will need to obtain permission directly from the copyright holder. To view a copy of this license, visit <http://creativecommons.org/licenses/by/4.0/>.

© The Author(s) 2019